Atmospheric
Measurement
Techniques

Open Access

Supplement of

Applications and limitations of constrained high-resolution peak fitting on low resolving power mass spectra from the ToF-ACSM

Hilkka Timonen et al.
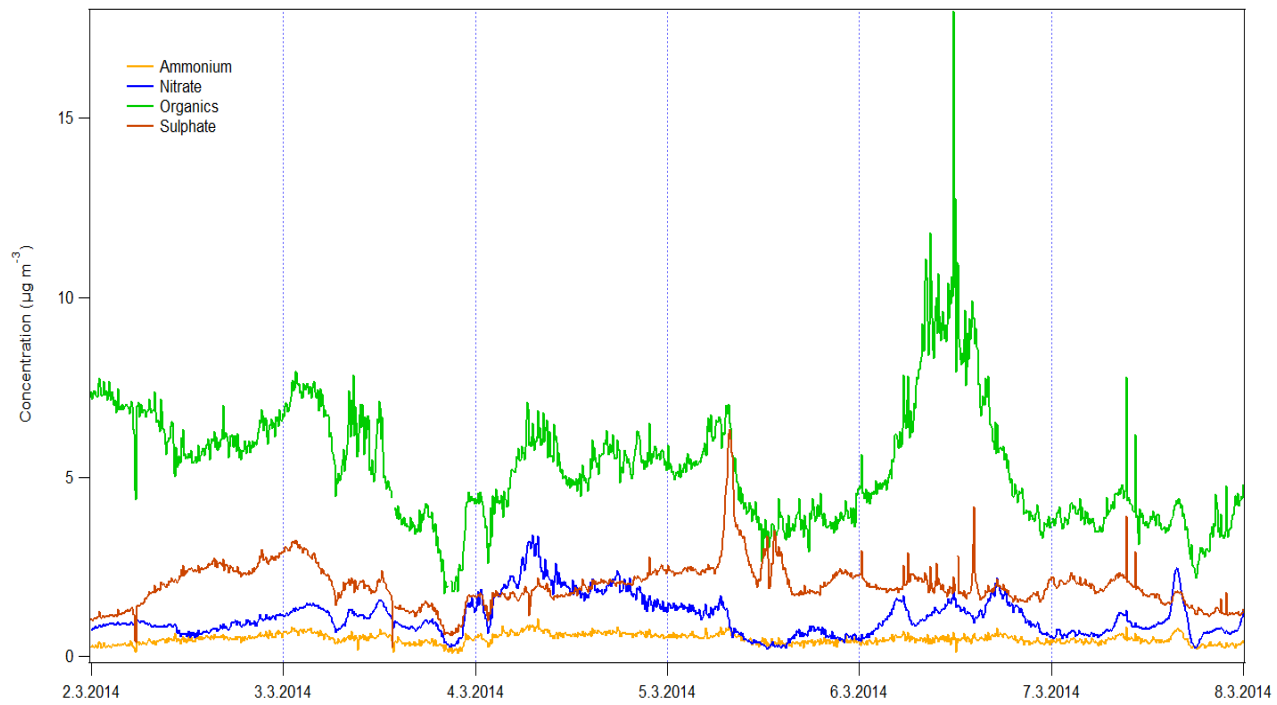
Correspondence to: Hilkka Timonen (hilkka.timonen@fmi.fi)

Figure S1: Time series of main ions measured at the SMEARIII station with a ToF-ACSM during the spring 2014 campaign.
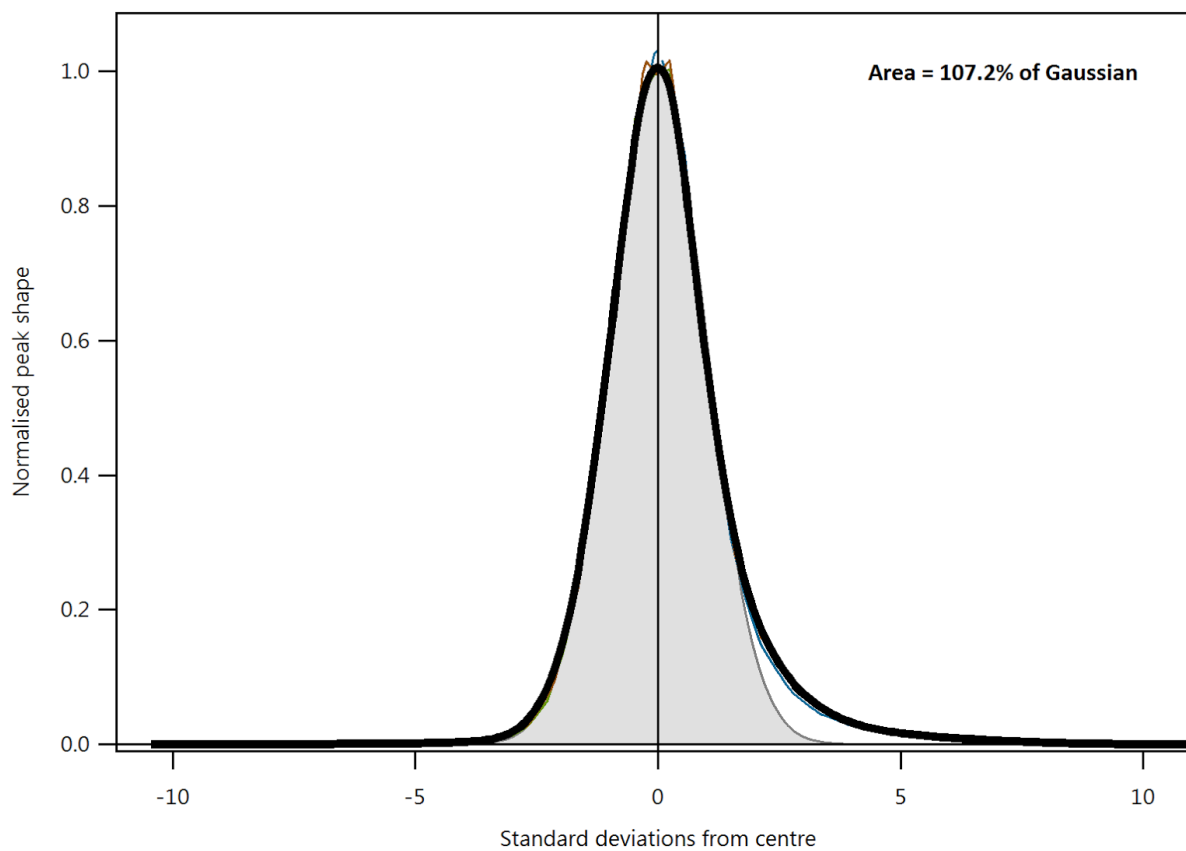
Area = 107.2% of Gaussian

Figure S2: The observed non-Gaussian peak shape calculated using a representative mass spectrum from the SMEARIII campaign data.
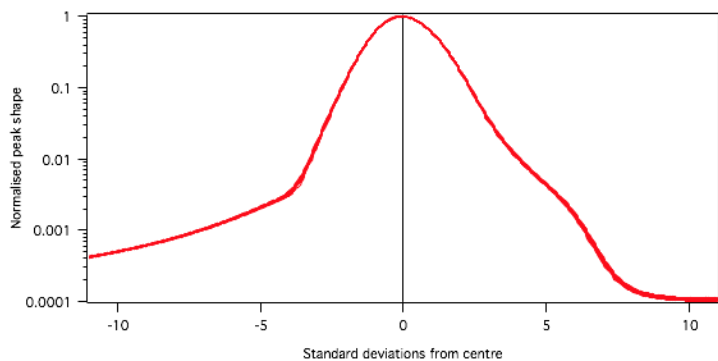
Figure S3: Normalised peak shape for the N_2^+ ion peak at 28 Th from 25 daily averages representing nearly a month of acquired data with consistent TOF tuning (voltages). No significant changes are observed over this time period, such that the individual traces are barely visible.
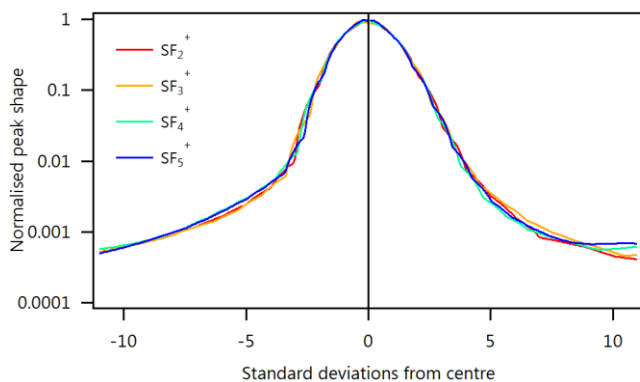

Figure S4: Normalised peak shape for various ions across a calibration MS with SF_6 gas: peak shape is consistent for the different SF_6 fragment ions and shows no obvious trend with mass-to-charge ratio.
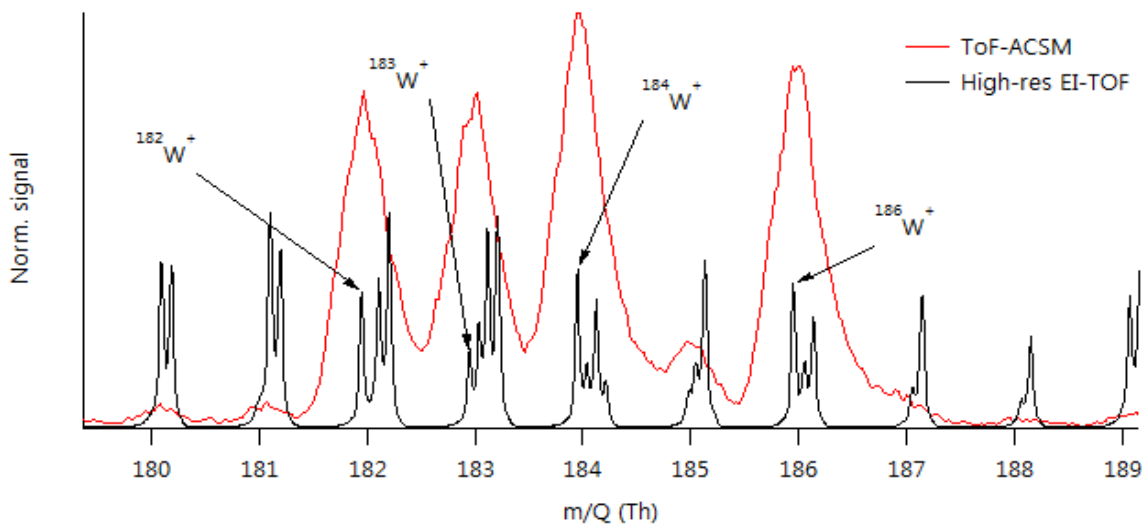
Figure S5: Comparison of a high-resolution EI-TOF MS with that from the ToF-ACSM. Note that the ToF-ACSM tungsten peaks are much stronger relative to the background than is observed in the EI-TOF. The multiple ions visible in the EI-TOF are measured as only single, broad, peaks in the ToF-ACSM.
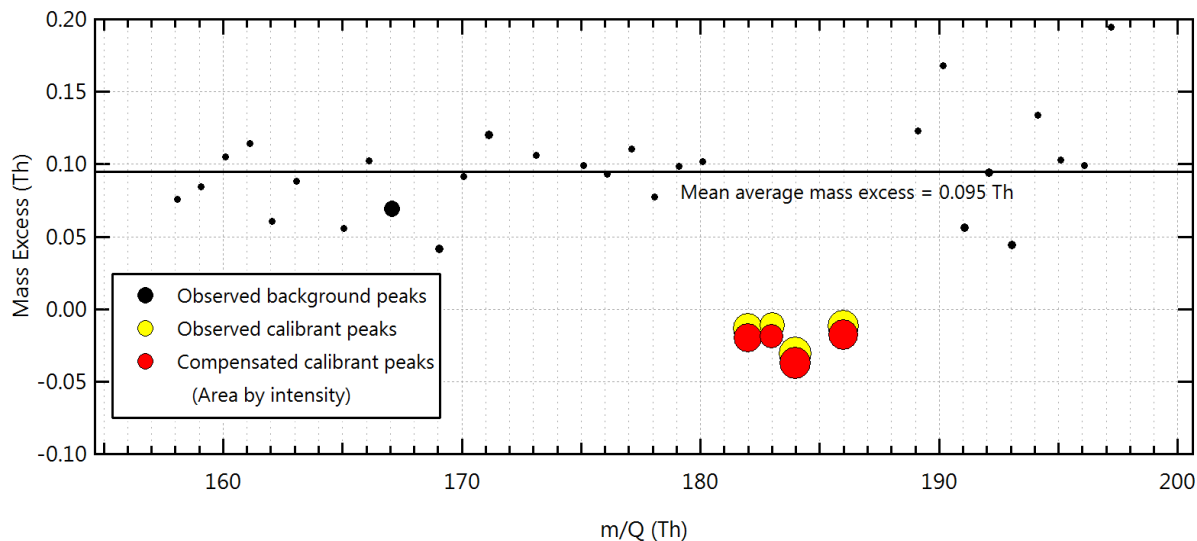

Figure S6: Compensating for the mass positions of calibrant peaks by assuming interferences are present of equal magnitude and mass excess to the surrounding isobaric peaks.
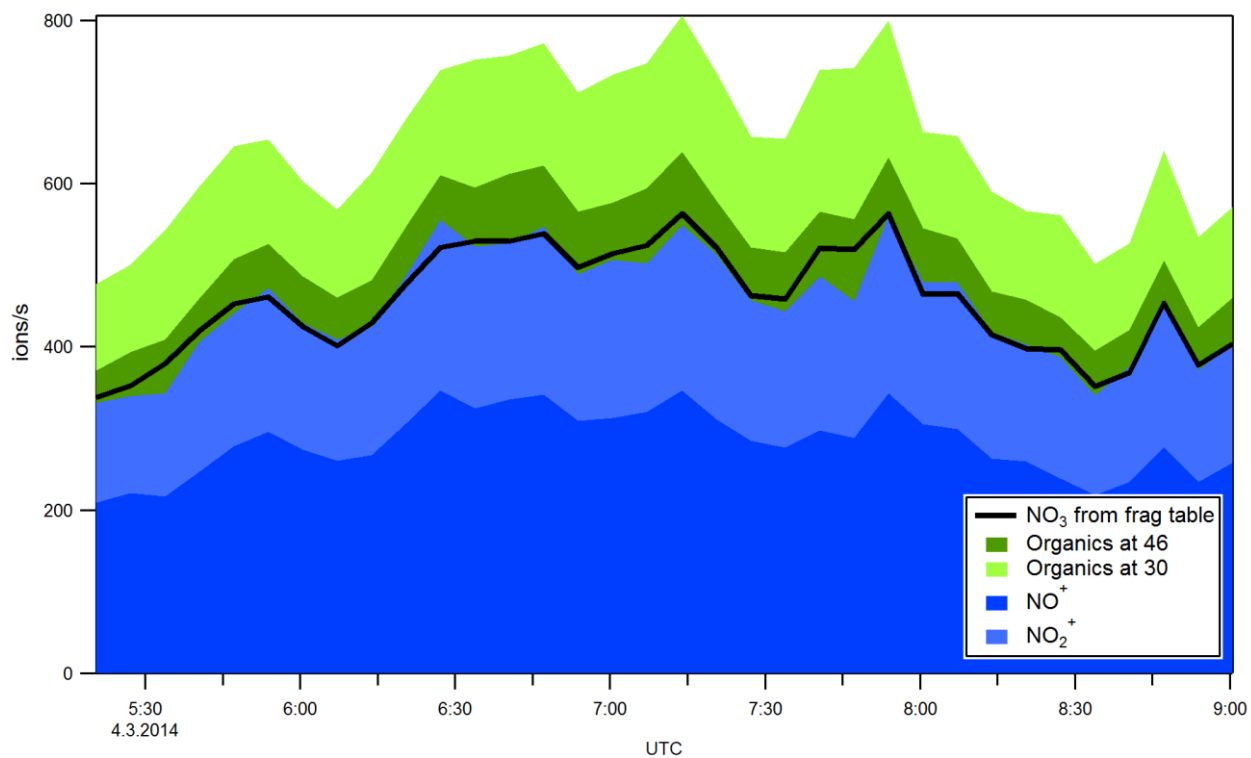
Fig S7: Time-series of the nitrate intensity derived from application of the fragmentation table to integrated (UMR) data compared to the sum of the fitted intensities for the nitrate ions NO^+ and NO_2^+ and their isobaric organic interferences. On average, the sum of NO^+ and NO_2^+ represents 102.7% of the integrated signal.
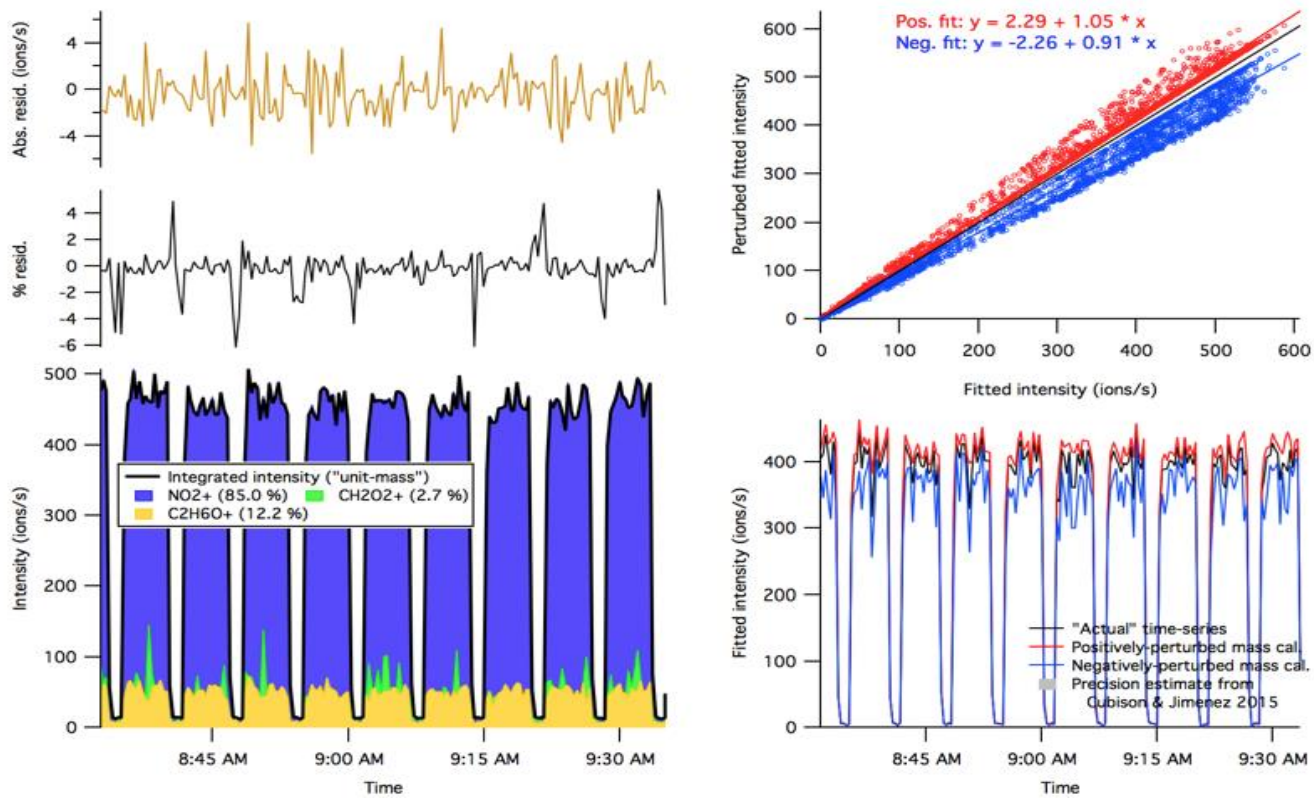
Figure S8: Sensitivity analysis for NO_2^+ using mass calibration perturbations of +/- 20 ppm.

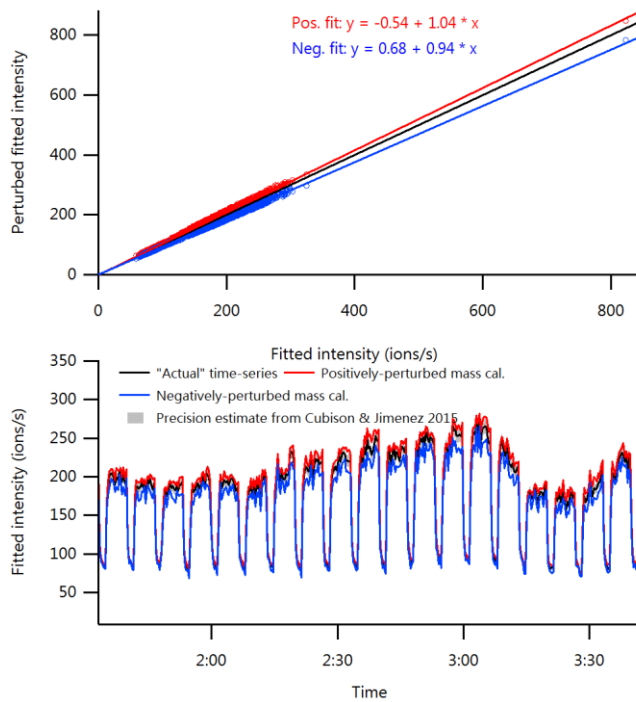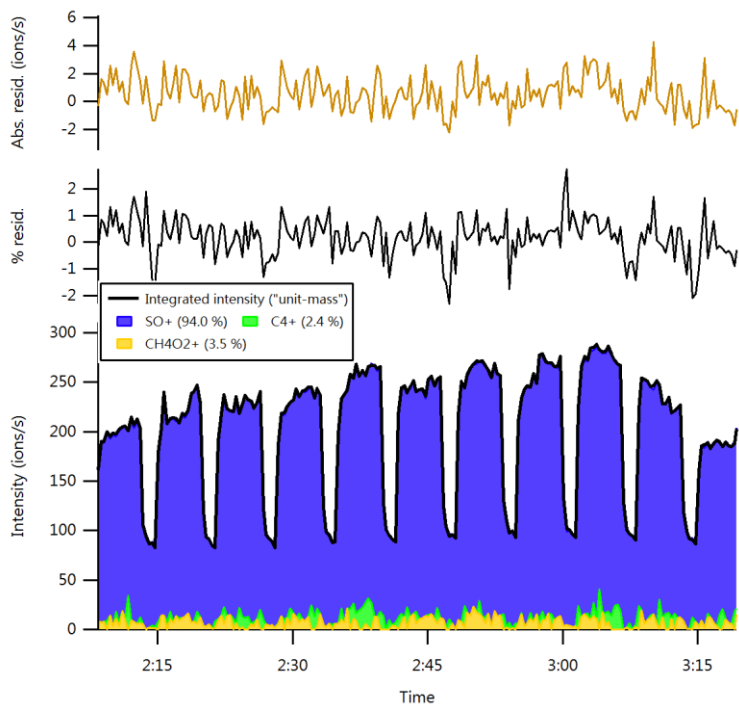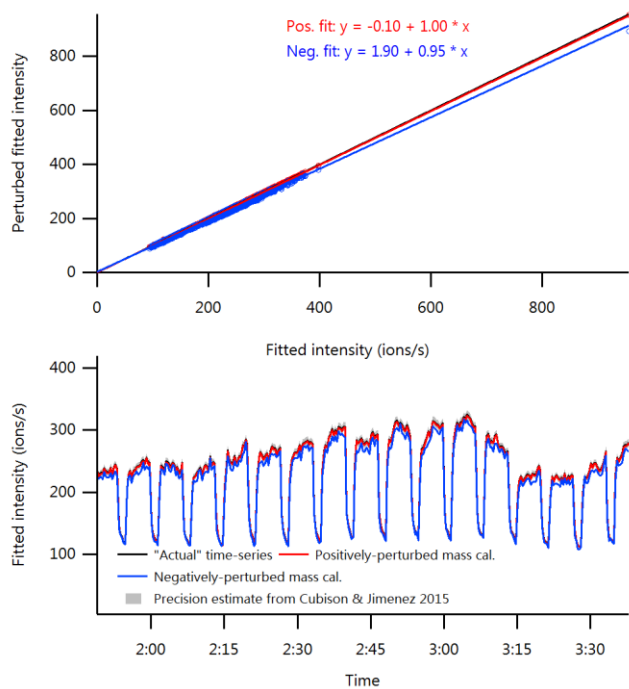Figure S9: Sensitivity analysis for SO$^+$ using mass calibration perturbations of +/- 20 ppm.
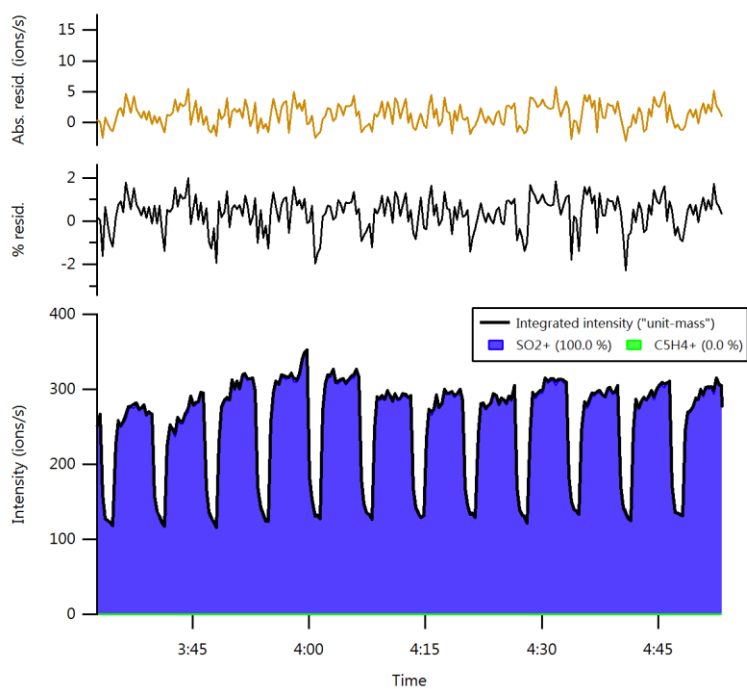
Figure S10: Sensitivity analysis for SO_2^+ using mass calibration perturbations of +/- 50 ppm.
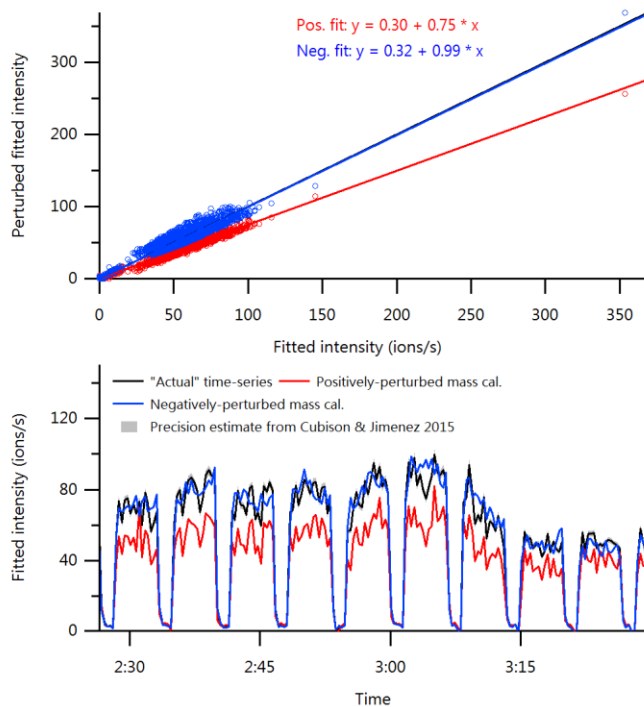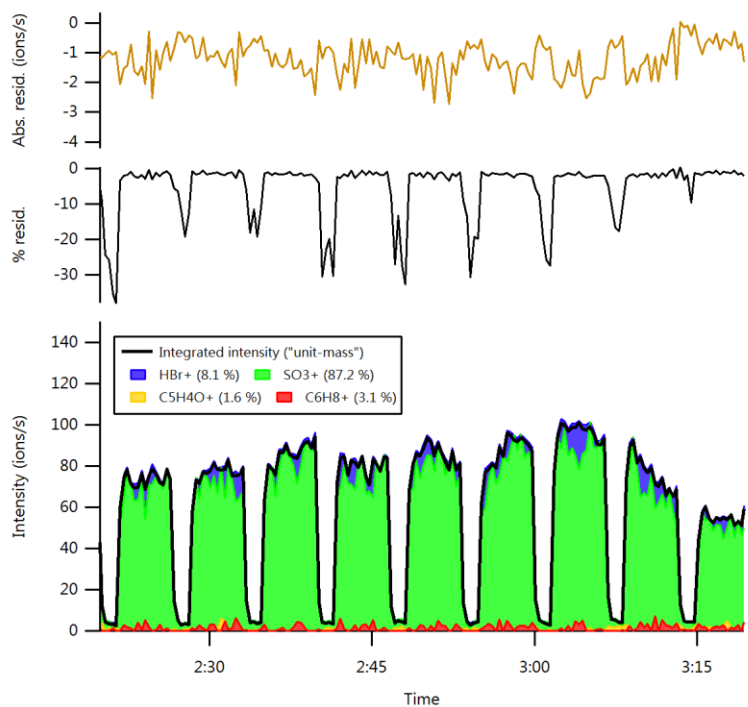
Figure S11: Sensitivity analysis for SO_3^+ using mass calibration perturbations of +/- 50 ppm.

Figure S12: Sensitivity analysis for HSO_3^+ using mass calibration perturbations of +/- 50 ppm.

Figure S13: Sensitivity analysis for $H_2SO_4^+$ using mass calibration perturbations of +/- 50 ppm.
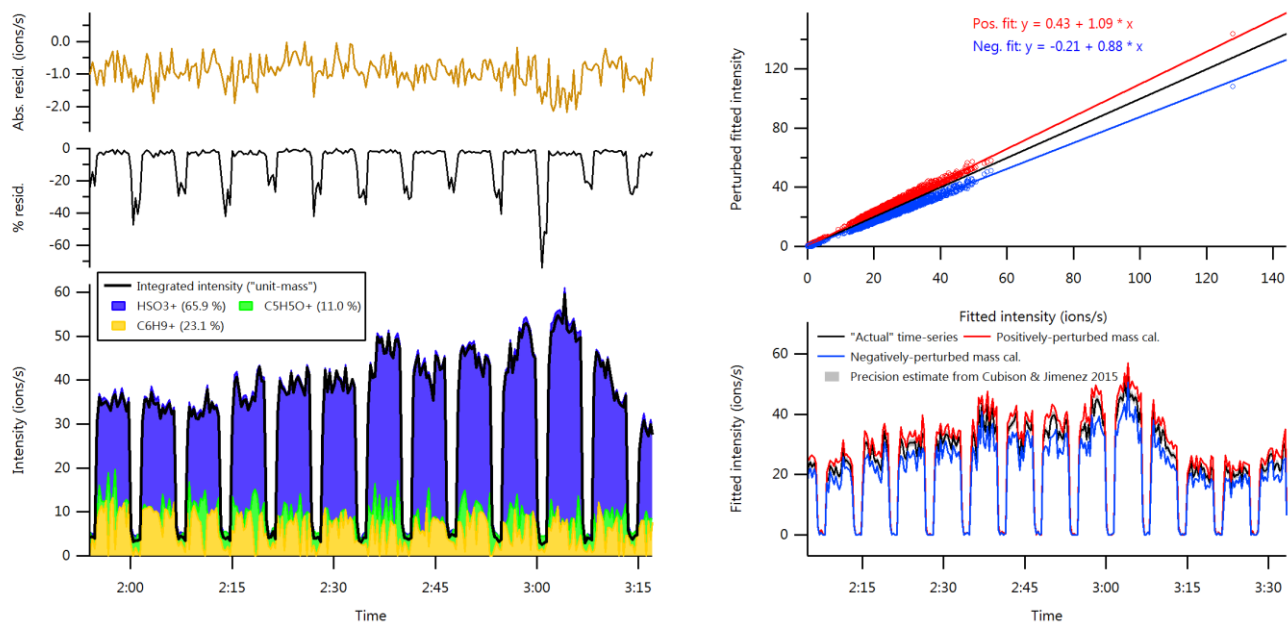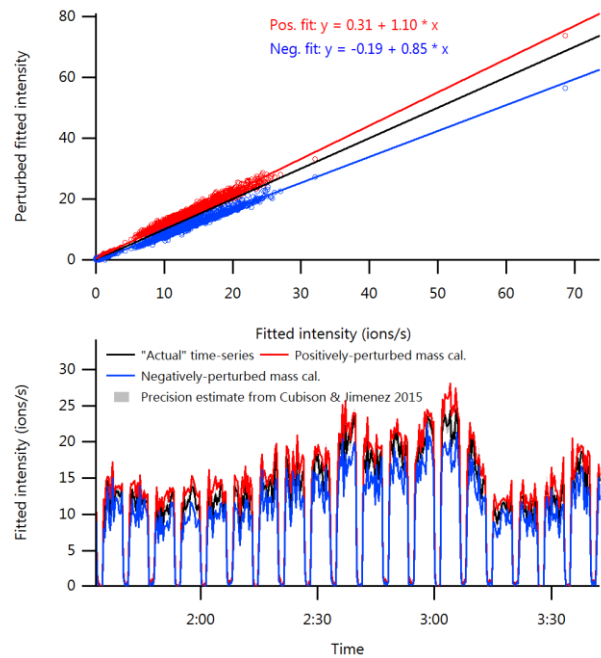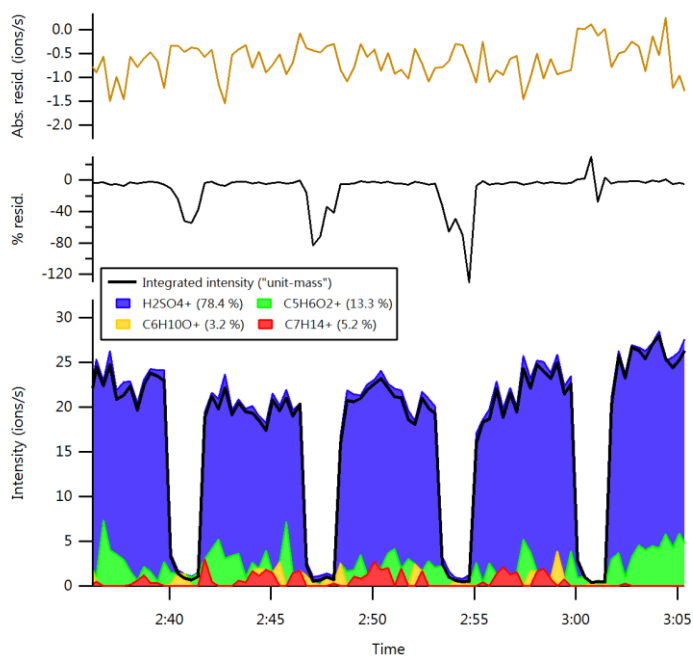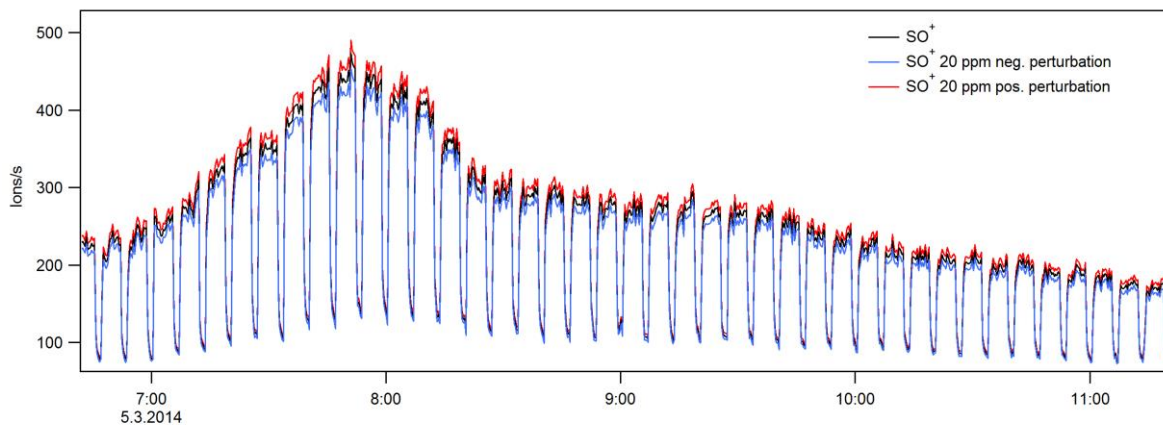
Figure S14: shows an example of positively and negatively perturbed time series for SO$^+$ -ion measured during the SMEARIII campaign. The difference between both negatively and positively perturbed and unperturbed time series was on average 4%.
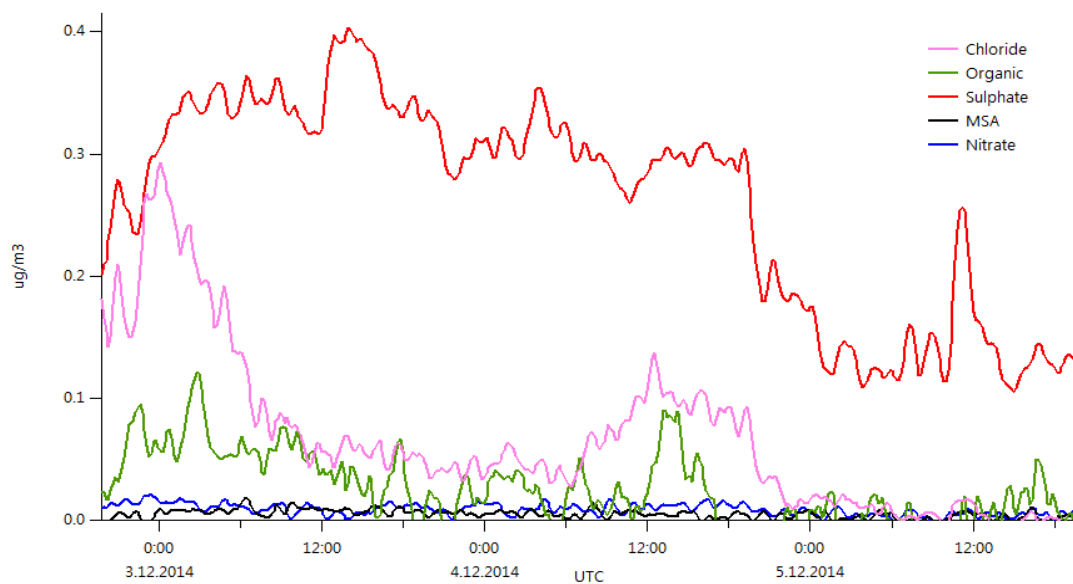
Figure S15: Time-series of ACSM species during episode 1 derived from integrated peak intensities observed with the ToF-ACSM at the Neumayer station at the beginning of December 2014.
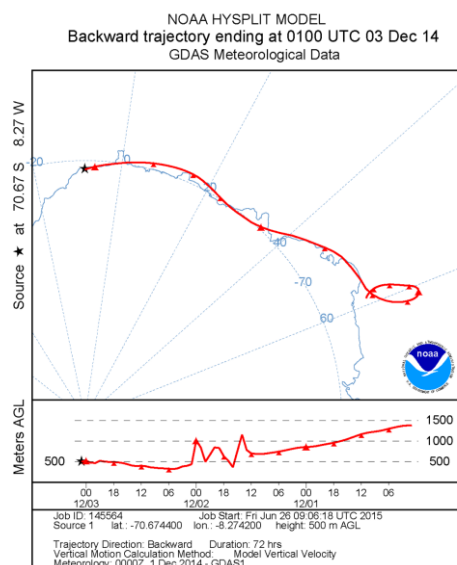

Figure S16: Airmass backtrajectory during episode 1 shows that air mass had transported in low altitude above sea area during last days before arriving to Neumayer station.
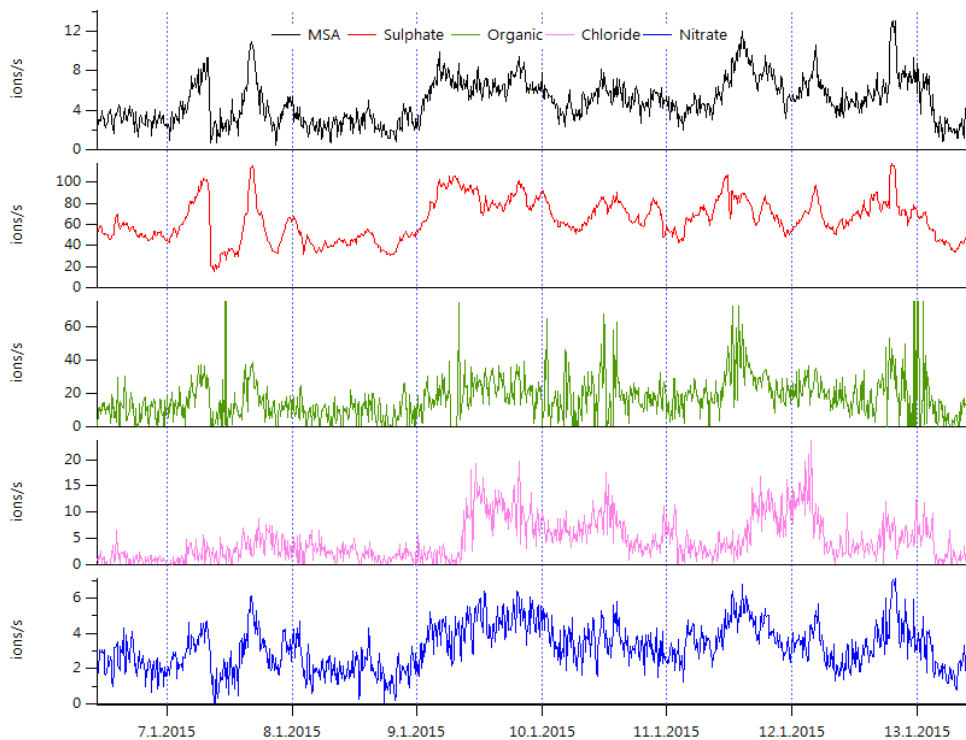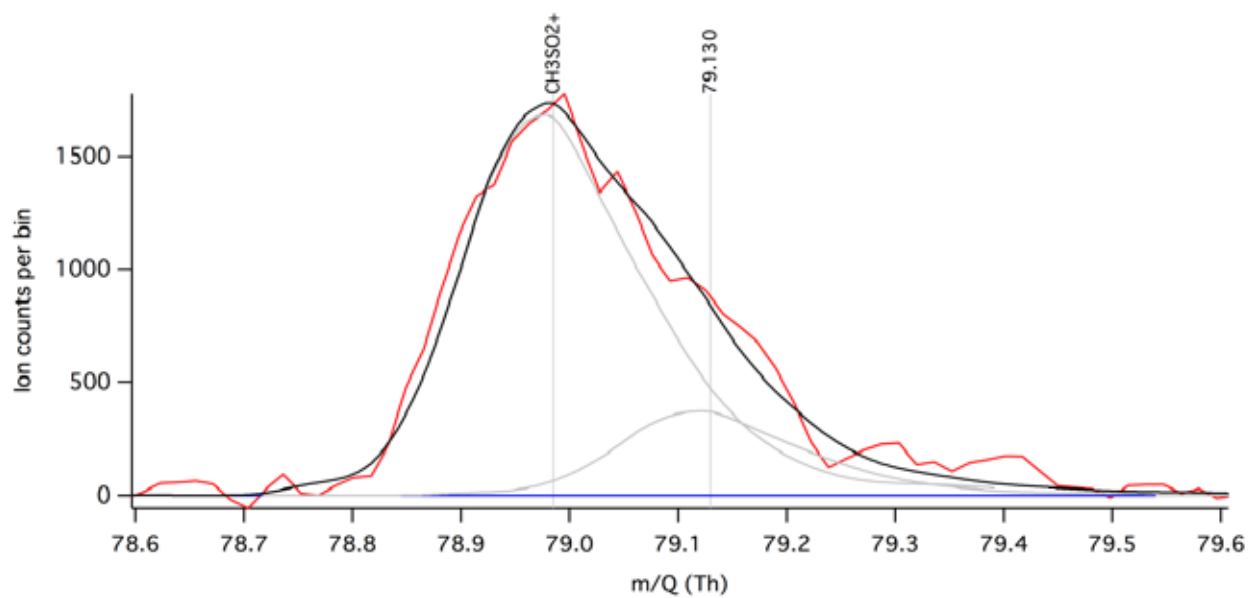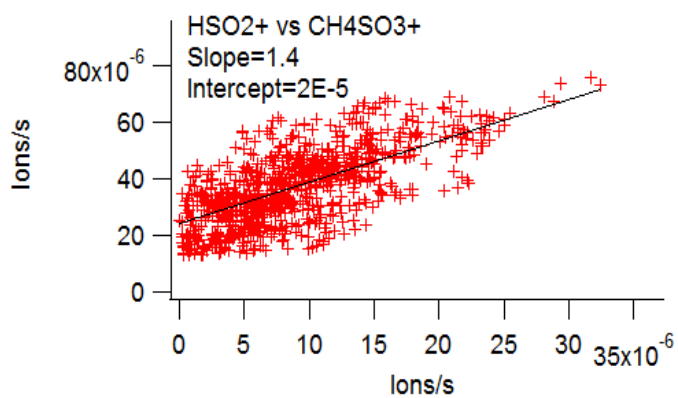
Figure S17: Time-series of ACSM species during episode 2 derived from integrated peak intensities observed with the ToF-ACSM at the Neumayer station in January 2015.

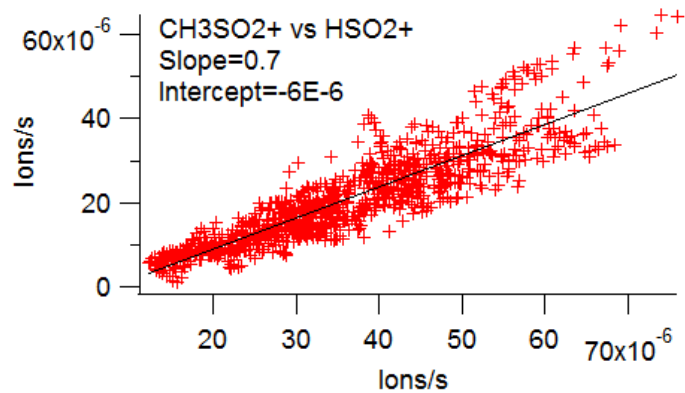FigureS18: Sensitivity of $CH_3SO_2^+$ to mass cal @ 100 ppm: 5%
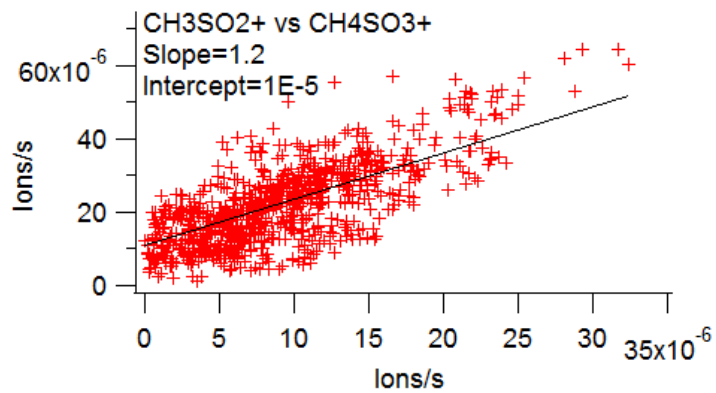-> clear that this peak is nearly all MSA.

Figure S19: Correlation between MSA main fragments a) HSO_2^+ vs $CH_4SO_3^+$, b)$CH_3SO_2^+$ vs HSO_2^+, c) $CH_3SO_2^+$ vs $CH_4SO_3^+$.

Table S1: Correlation (Pearson correlation r) between all fragments associated with the MSA

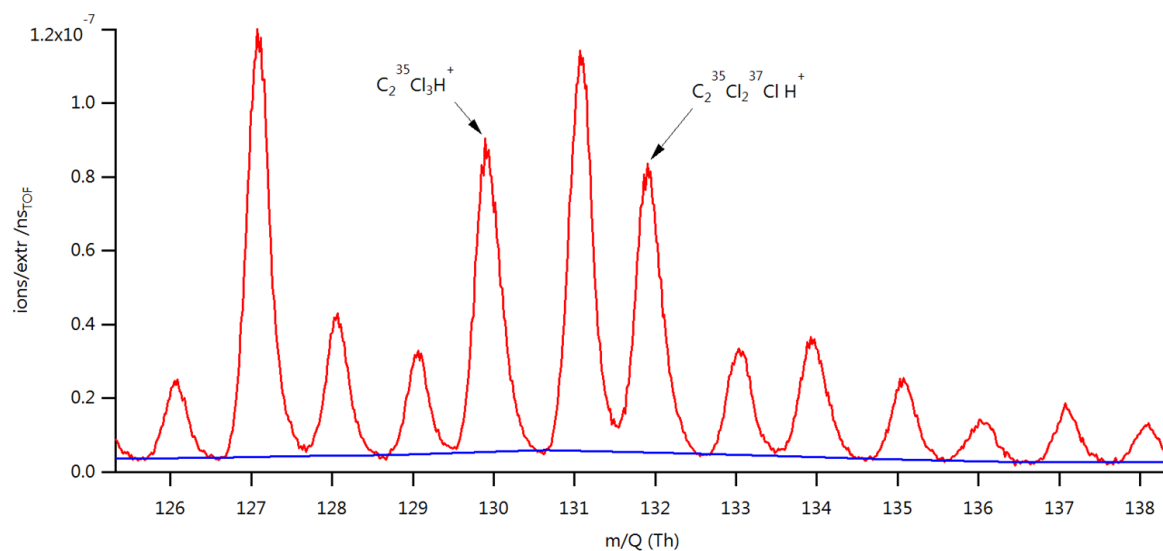|	CH3S+	CHS+	CH2SO2+	CH3SO2+	HSO2+	CH4SO3+
CH3S+	1					
CHS+	0.061827	1				
CH2SO2+	0.135439	0.294476	1			
CH3SO2+	0.237239	0.446346	0.696882	1		
HSO2+	0.265439	0.36614	0.598735	**0.892511**	1	
CH4SO3+	0.232336	0.333807	0.534572	**0.742081**	**0.719259**	1

Figure S20: Example MS showing the trichloroethylene peaks with assumed overlapping interferences from organic background ions. The mass defect at 130 and 132 Th is visibly more negative than at the surrounding peaks.
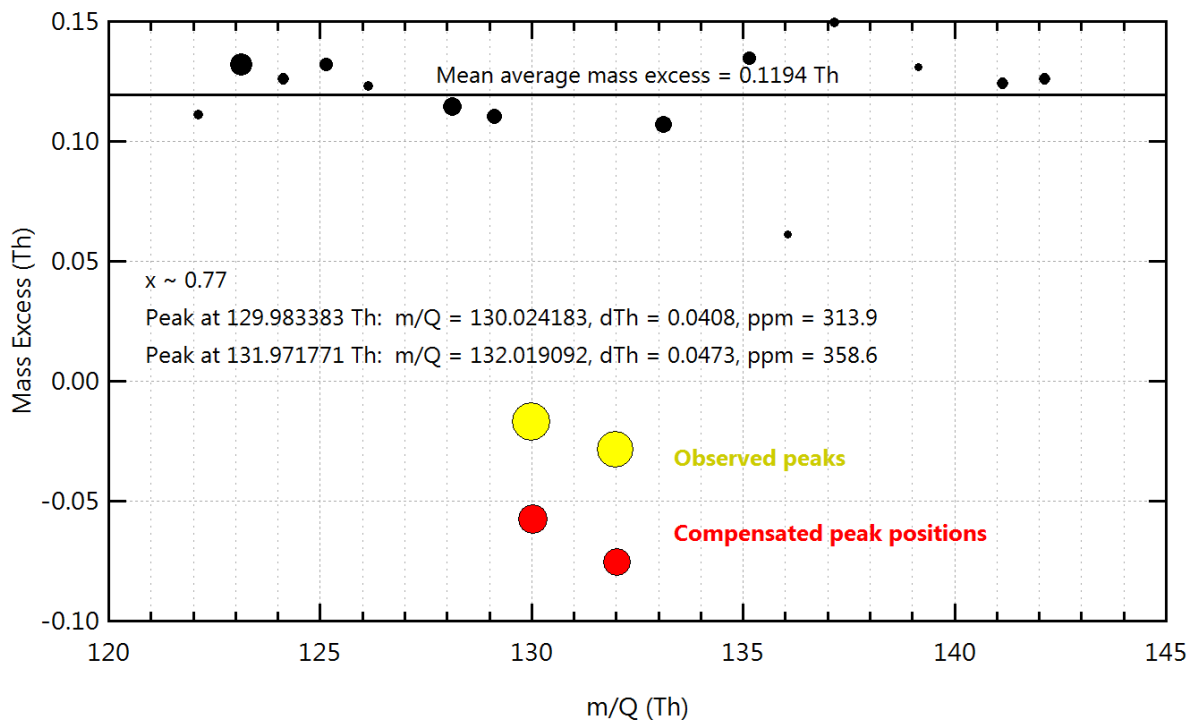
Fig S21: Compensating for the mass positions of calibrant peaks by assuming interferences are present of equal magnitude and mass defect to the surrounding isobaric peaks.
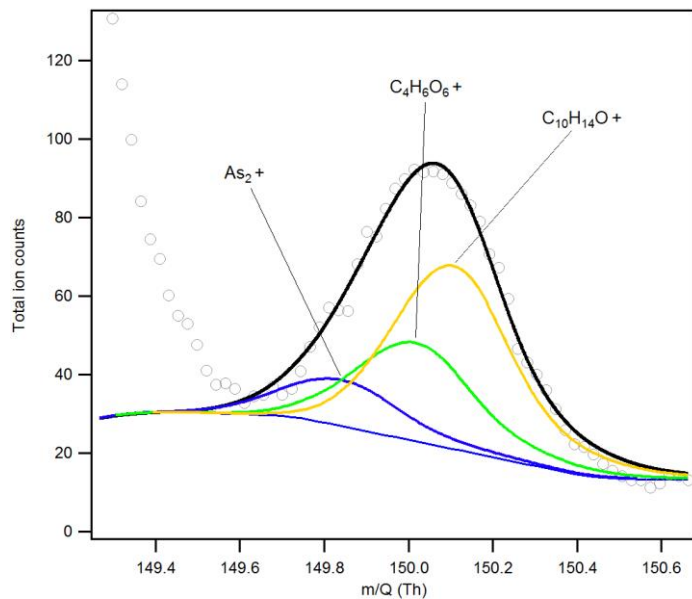

Figure S22: Example mass spectrum showing the HR fits for As_2^+ and the organic background peaks at 150 Th.
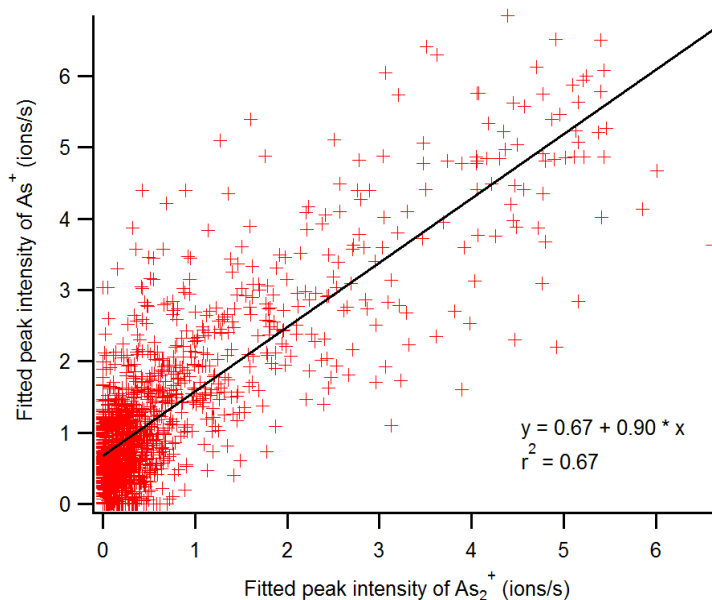
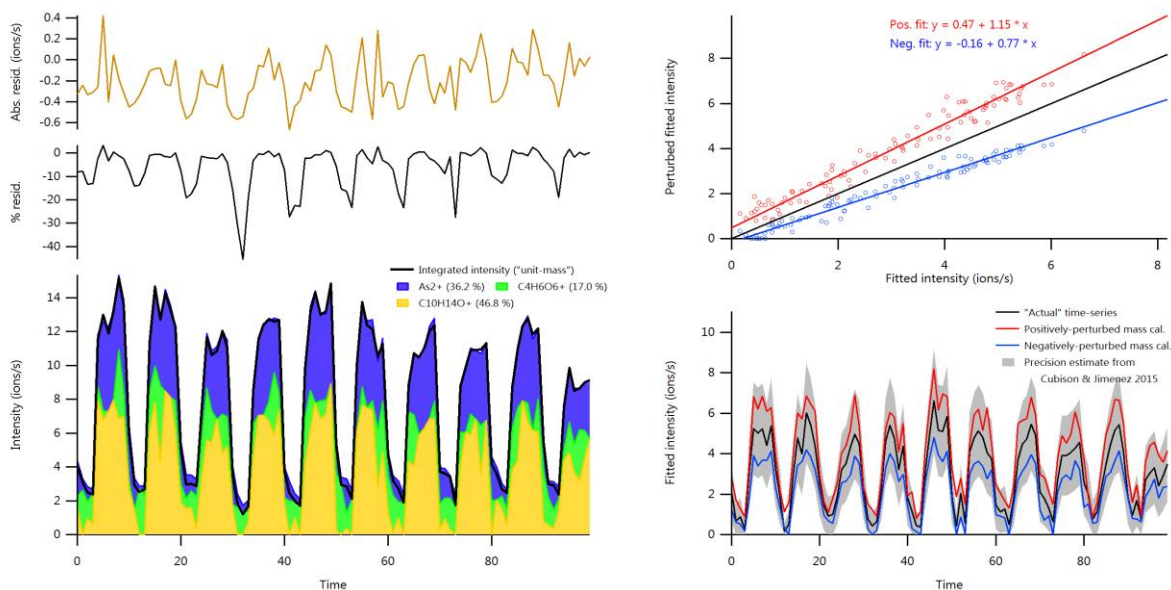Figure S23: Scatter plot of the fitted peak intensities for As$^+$ and As$_2$$^+$.

Figure S24: Assessing the sensitivity of the fitted peak intensity of the As$_2$$^+$ ion to perturbations in the mass calibration of +/- 200 ppm. Left: the sum of the ions fitted at this peak compared with the integrated signal (bottom) and the absolute and relative residuals (top). Top right: Scatter plots of the fitted As$_2$$^+$ signals for the perturbed vs best-case mass calibration scenarios. Bottom right: Time-series of the fitted As$_2$$^+$ intensities, with the perturbed mass calibration cases shown in red and blue. The shading around the black line indicates the expected precision predicted by the parameterisation of Cubison and Jimenez (2015).
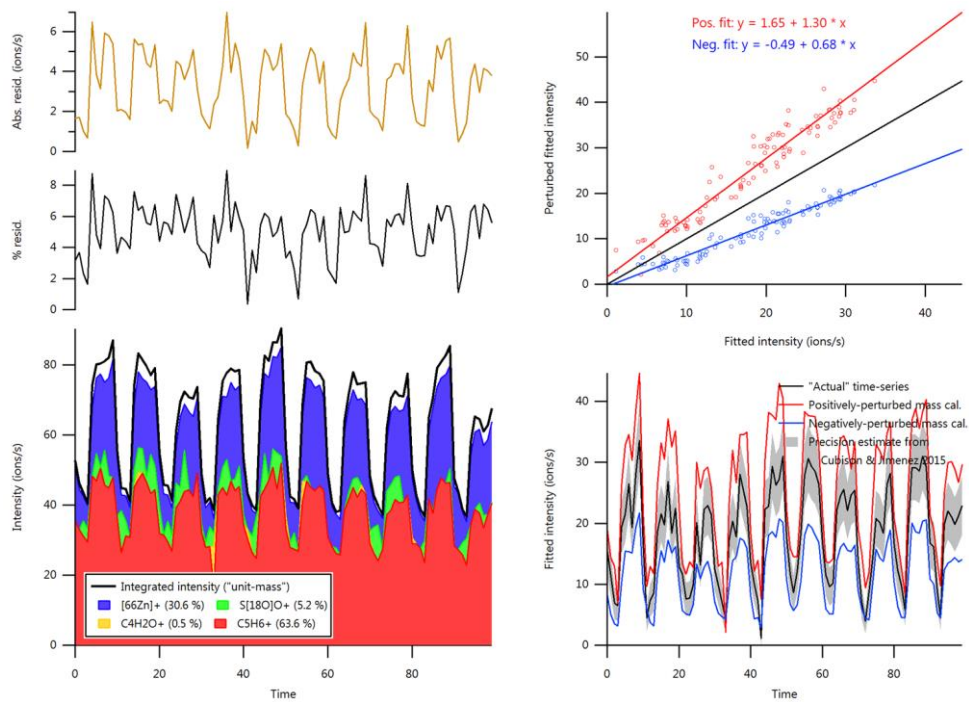
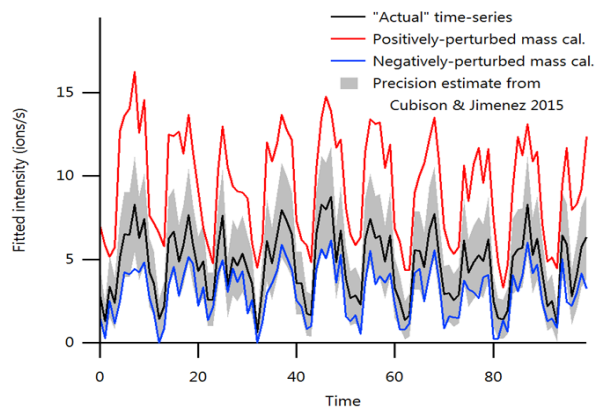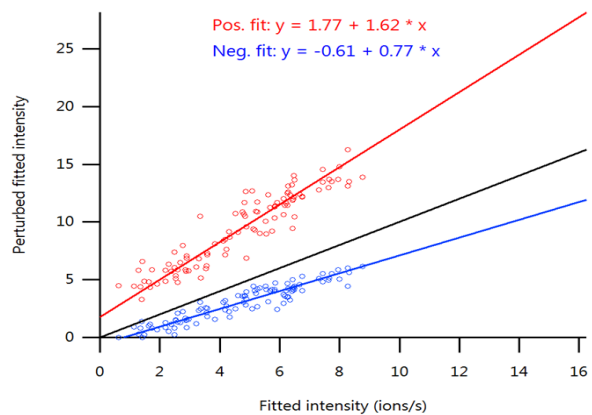Figure S25: Sensitivity analysis of peak-fitting at 66 Th showing a non-zero contribution from the ion $^{66}Zn^+$.
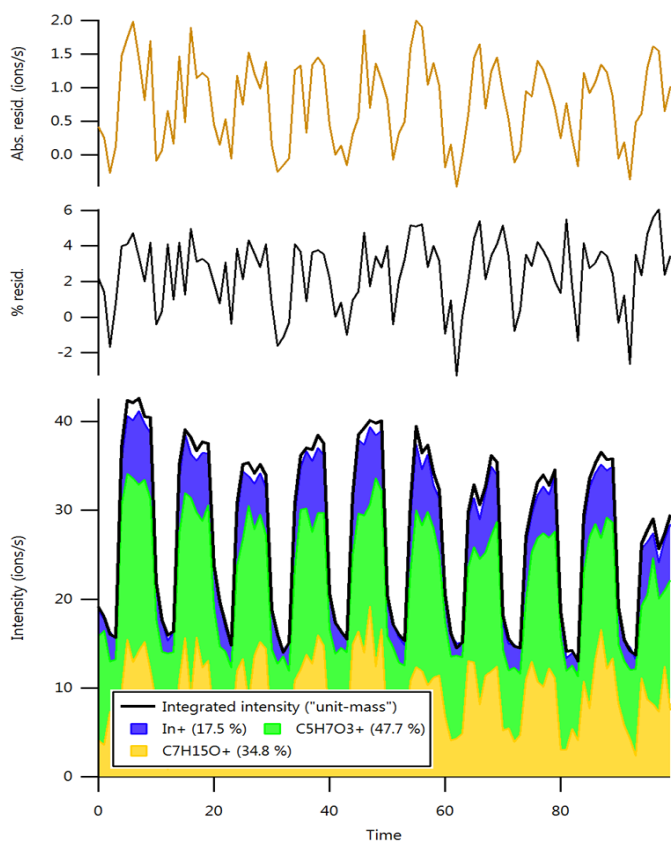
Figure S26: Sensitivity analysis of peak-fitting at 115 Th showing a weak but non-zero contribution from the ion In$^+$.
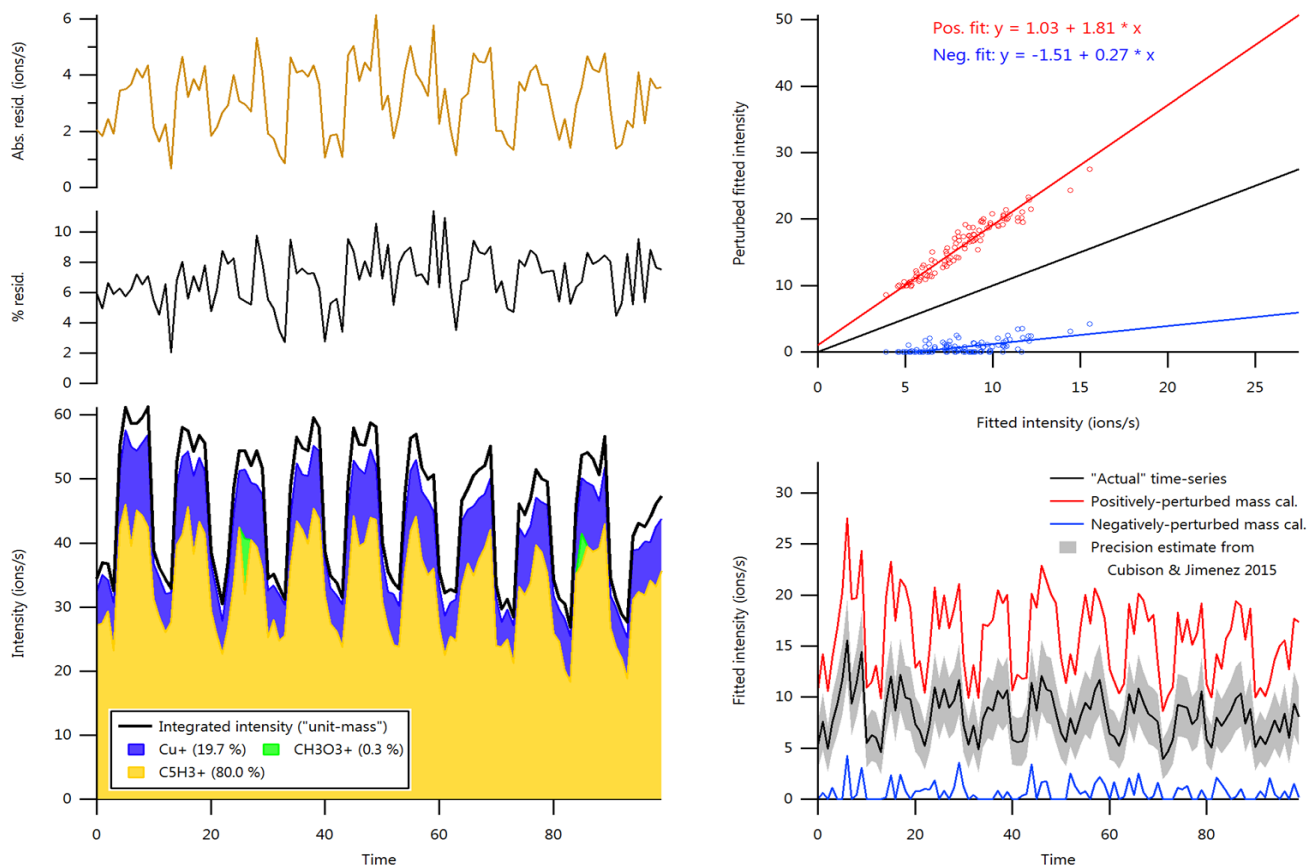
Figure S27: Sensitivity analysis of peak-fitting at 63 Th showing high sensitivity of the fitted intensity of the Cu^+ ion to mass calibration.
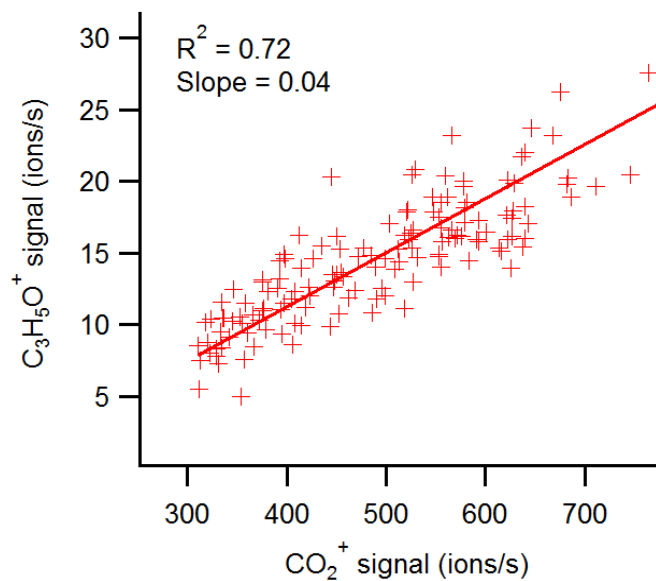
Figure S28: Scatter plot of the difference signal for the fitted intensities of the $C_3H_5O^+$ and CO_2^+ ions.

Parameterisation of Stark et al. (2015) for the calculation of carbon oxidation state from mass excess (ME):

$$OSc = A*ME + B*m/Q + C*[ME / (m/Q)] + D$$

where A = 2.796, B = -1.304e-3, C = -4.05e3, D = 1.295